Numerical Heat Transfer, Part B, 66: 526–543, 2014

ISSN: 1040-7790 print/1521-0626 online
DOI: 10.1080/10407790.2014.894372

Taylor & Francis
Taylor & Francis Group

DEVELOPMENT OF A NOVEL FULLY COUPLED SOLVER IN OPENFOAM: STEADY-STATE INCOMPRESSIBLE TURBULENT FLOWS IN ROTATIONAL REFERENCE FRAMES

L. Mangani[1], M. Buchmayr[2,3], and M. Darwish[4]
[1]*Hochschule Luzern, Technik und Architektur, Horw, Switzerland*
[2]*Andritz AG, Graz, Austria*
[3]*Department of Thermal Turbomachinery, TU Graz, Graz, Austria*
[4]*Department of Mechanical Engineering, American University of Beirut, Beirut, Lebanon*

In this article, the fully coupled block algorithm for the solution of three-dimensional incompressible turbulent flows presented in a companion article [1] is extended for use with multiple reference frames and multiple mesh blocks. The implicit block coupling is applied to the extra rotational terms, and to the multiblock interfaces. Furthermore, implementation details on the linearization of cyclic and other boundary conditions are detailed. These modifications allow the coupled solver to retain its improved performance and robustness in addition to mesh size scalability while solving turbomachinery-type applications. The performance and mesh size scalability of the coupled solver is compared to that of a segregated pressure based solver [2] using three industrial-size test cases.

1. INTRODUCTION

In a companion article [1], the authors demonstrated the advantages of using a fully implicit coupled approach in resolving the pressure–momentum coupling that arises in the Navier-Stokes equations, namely, better performance, improved robustness, and near-linear mesh scalability. This was demonstrated by solving four test problems on increasingly refined meshes. Mesh scalability was defined as the characteristic of an algorithm to have its computational cost increase linearly with mesh size. Similar procedures of pressure-based algorithms for unstructured grids have been outlined by Laia et al. [3] and Woodfield et al. [4], and block-coupled solution techniques have been reported by Vradis et al. [5] and De Lemos et al. [6]. In this article the fully implicit coupled algorithm presented in the companion artice [1] is extended to allow for the solution of turbulent problems with multiblock meshes in multiple reference frames (MRF), a feature that is critical for the simulation of

Received 13 November 2013; accepted 25 January 2014.
Address correspondence to L. Mangani, Hochschule Luzern, Technik und Architektur, Horw, Switzerland. E-mail: luca.mangani@hslu.ch
Color versions of one or more of the figures in the article can be found online at www.tandfonline.com/unhb.

NOMENCLATURE

$\mathbf{A}$, a	coefficient matrix, coefficient matrix coefficient
AMI	arbitrary mesh interface
$\mathbf{b}$, b	source vector, source vector coefficient
CV	control volume
$\mathbf{D}$	Rhie-Chow numerical dissipation tensor
g	geometric interpolation weighting factor
k	turbulence kinetic energy
max	maximum of two values
min	minimum of two values
p	pressure
res	residual vector
RMS	normalized root-mean-square of residual vector
S, $\mathbf{S}$	surface scalar, surface normal vector
$time$	calculation time
u, v, w	velocity components
$\mathbf{u}$	velocity vector
V, $\dot{V}$	volume scalar, volume flux scalar
ν	kinematic viscosity scalar
ρ	density constant
ϕ	general quantity
ω	turbulence frequency or unit rotation vector
Ω	angular velocity of rotating frame

Subscripts

C	cell under consideration
$conv$	refers to convection term
eff	refers to effective turbulence viscosity
$geom$	refers to geometric transformation
NB	neighbor cell of cell under consideration
$nCells$	total number of cells in calculation domain
r	refers to rotational frame of reference
ref	reference
rot	refers to rotational term
$wall$	refers to quantities at wall boundary

Superscripts

n	current iteration
$\underline{u}$, $\underline{v}$, $\underline{w}$	refers to velocity components
$\overline{\phi}$	linear interpolation to the face

turbomachinery applications. To preserve the convergence behavior and scalability, it is essential to use a fully implicit treatment for the multiblock interfaces, whether with conforming or nonconforming meshes. To this end, the implicit multiblock procedure of Darwish et al. [7] was adopted. Since turbomachinery flows are generally turbulent, the k–ω SST turbulence model [8] is used with the coupled solver.

In the remainder of the article the governing equations in a rotating reference frame are first presented, then the key features of the MRF coupled solver are detailed, namely, the implicit discretisation of the rotational terms, the arbitrary mesh interface (AMI) interblock interface, the cyclic patches, and other boundary conditions. Finally, the performance and mesh scalability of the algorithm are evaluated for a variety of industrial turbomachinery applications.

2. GOVERNING EQUATIONS

In a rotating reference frame with constant angular velocity ($\dot{\mathbf{\Omega}} = 0$), the Navier-Stokes equations for steady flows can be reformulated as [9]

$$\nabla \cdot \mathbf{u_r} = 0 \tag{1}$$

$$\nabla \cdot (\mathbf{u_r}\mathbf{u_r}) + 2\Omega \times \mathbf{u_r} + \Omega \times \Omega \times \mathbf{r} = -\frac{1}{\rho}\nabla p + \nabla \cdot \left(\nu_{eff}(\nabla \mathbf{u})\right) \tag{2}$$

where Ω is the angular velocity of the rotating frame, and $\mathbf{u_r}$ is the relative velocity in the rotational system. The absolute or stationary frame velocity, $\mathbf{u}$, is written

$$\mathbf{u} = \mathbf{u_r} + \Omega \times \mathbf{r} \tag{3}$$

In Eq. (2) the second and third terms are the Coriolis and centripetal forces, respectively.

To facilitate the numerical discretization and resolution of these equations in multiple rotating frames, the equations are re-cast in terms of the stationary, or absolute, velocity [10], yielding

$$\nabla \cdot \mathbf{u} = 0 \tag{4}$$

$$\nabla \cdot (\mathbf{u_r u}) + \Omega \times \mathbf{u} = -\frac{1}{\rho}\nabla p + \nabla \cdot \left[\nu_{eff}(\nabla \mathbf{u})\right] \tag{5}$$

In Eq. (5) the effective kinematic viscosity is the sum of the laminar and turbulent kinematic viscosities ($\nu_{eff} = \nu + \nu_t$). The convecting flux is written in terms of the relative velocity while the convected velocities are expressed in the stationary frame. As in Eq. (3), the relation between the relative volume flux $\dot{V}_r$ and absolute volume flux $\dot{V}$ can be written as

$$\dot{V} = \dot{V}_r + (\Omega \times \mathbf{r}) \cdot \mathbf{S}_f \tag{6}$$

In a rotational reference frame the k–ω SST turbulence model becomes

$$\nabla \cdot (\mathbf{u}_r k) - \nabla \cdot [(\nu + \nu_t \alpha_K)\nabla k] = \frac{1}{\rho} P_k - \beta^* \omega k \tag{7}$$

$$\nabla \cdot (\mathbf{u}_r \omega) - \nabla \cdot [(\nu + \nu_t \alpha_\omega)\nabla \omega] = \frac{C_1 P_k}{\mu_t} - C_2 \omega^2 + \frac{2\alpha_\varepsilon (1 - F_1)}{\omega} \nabla k \cdot \nabla \omega \tag{8}$$

In Eqs. (7) and (8) the effects of curvature or rotation [11, 12] are not accounted for.

3. DISCRETIZATION

With much of the details of the fully implicit coupling algorithm already presented in the companion article [1], the focus of our numerical derivations is on the discretization of the key features of MRF flows. The starting point is the block coefficient matrix derived in the companion article [1],

$$\begin{bmatrix} a_C^{uu} & a_C^{uv} & a_C^{uw} & a_C^{up} \\ a_C^{vu} & a_C^{vv} & a_C^{vw} & a_C^{vp} \\ a_C^{wu} & a_C^{wv} & a_C^{ww} & a_C^{wp} \\ a_C^{pu} & a_C^{pv} & a_C^{pw} & a_C^{pp} \end{bmatrix} \cdot \begin{bmatrix} u_C \\ v_C \\ w_C \\ p_C \end{bmatrix} + \sum_{NB} \begin{bmatrix} a_{NB}^{uu} & a_{NB}^{uv} & a_{NB}^{uw} & a_{NB}^{up} \\ a_{NB}^{vu} & a_{NB}^{vv} & a_{NB}^{vw} & a_{NB}^{vp} \\ a_{NB}^{wu} & a_{NB}^{wv} & a_{NB}^{ww} & a_{NB}^{wp} \\ a_{NB}^{pu} & a_{NB}^{pv} & a_{NB}^{pw} & a_{NB}^{pp} \end{bmatrix} \cdot \begin{bmatrix} u_{NB} \\ v_{NB} \\ w_{NB} \\ p_{NB} \end{bmatrix} = \begin{bmatrix} b_C^u \\ b_C^v \\ b_C^w \\ b_C^p \end{bmatrix} \tag{9}$$

The discretization of the rotational term, the linearization of some boundary conditions such as the no-slip wall and the cyclic patch, and the implementation of the arbitrary mesh interfaces (Section 3.4) will now be detailed.

3.1. Rotational Term

In the momentum equation (5), the rotational term $\Omega \times \mathbf{u}$ is discretized implicitly by integrating it over a control volume and adding the resulting coefficient to the diagonal matrix, yielding

$$\begin{aligned} a^{uv}_{C,rot} &= -\Omega_z \, \Delta V & a^{uw}_{C,rot} &= \Omega_y \, \Delta V \\ a^{vu}_{C,rot} &= \Omega_z \, \Delta V & a^{vw}_{C,rot} &= -\Omega_x \, \Delta V \\ a^{wu}_{C,rot} &= -\Omega_y \, \Delta V & a^{wv}_{C,rot} &= \Omega_x \, \Delta V \end{aligned}$$

For convection in a rotational reference frame, the convecting flux is defined in terms of the relative volume flux, thus the convection term coefficients become

$$\begin{aligned} a^{uu}_{C,conv} &= |\dot{V}^n_r, 0| & a^{uu}_{NB,conv} &= -|-\dot{V}^n_r, 0| \\ a^{vv}_{C,conv} &= |\dot{V}^n_r, 0| & a^{vv}_{NB,conv} &= -|-\dot{V}^n_r, 0| \\ a^{ww}_{C,conv} &= |\dot{V}^n_r, 0| & a^{ww}_{NB,conv} &= -|-\dot{V}^n_r, 0| \end{aligned}$$

3.2. Moving-Wall Boundary Condition

Boundary conditions for coupled solvers do not differ from those of segregated algorithms. This is the case for both Dirichlet and von Neumann types of boundary conditions. However, it is critical to ensure that the coefficients are linearized whenever possible. This can be done in the coupled solver since the nondiagonal elements can be resolved into the inter-equation coupling coefficients. This is illustrated for the shear stress at moving walls.

At rotating walls the rotational volume flux $\dot{V}_r$ over the boundary face is zero. Hence the contribution of the convection term in the momentum equations will be zero.

Following [13], the shear force reads

$$\mathbf{F}_{b,shear} = \tau_b \, \|\mathbf{S}_f\| \tag{10}$$

with the shear stress at the boundary being

$$\frac{\tau_b}{\rho} = -\nu \frac{\partial \mathbf{u}}{\partial \mathbf{n}} \tag{11}$$

For moving-wall discretization this yields

$$\frac{\tau_b}{\rho} = -\nu \frac{\mathbf{u}_{\parallel,C} - \mathbf{u}_{\parallel,wall}}{d_\perp} \tag{12}$$

The velocity at the cell center adjacent to the boundary is not necessarily tangential to the wall, however only its tangential component $\mathbf{u}_{\parallel,C}$ contributes to the shear stress. The parallel velocity vector, as seen in Figure 1 can be written as

$$\mathbf{u}_\parallel = \mathbf{u} - \underbrace{(\mathbf{u} \cdot \mathbf{n}_b)\mathbf{n}_b}_{\mathbf{u}_\perp} \tag{13}$$

which upon substitution into Eq. (11) and linearization yields the following coefficients

$$\begin{aligned}
a^{uu}_{C,b} &= \frac{\nu \|\mathbf{S}_b\|}{d_\perp}\left(1 - n^2_{b,x}\right) & a^{uv}_{C,b} &= -\frac{\nu \|\mathbf{S}_b\|}{d_\perp} n_{b,x} n_{b,y} & a^{uw}_{C,b} &= -\frac{\nu \|\mathbf{S}_b\|}{d_\perp} n_{b,x} n_{b,z} \\
a^{vu}_{C,b} &= -\frac{\nu \|\mathbf{S}_b\|}{d_\perp} n_{b,y} n_{b,x} & a^{vv}_{C,b} &= \frac{\nu \|\mathbf{S}_b\|}{d_\perp}\left(1 - n^2_{b,y}\right) & a^{vw}_{C,b} &= -\frac{\nu \|\mathbf{S}_b\|}{d_\perp} n_{b,y} n_{b,z} \\
a^{wu}_{C,b} &= -\frac{\nu \|\mathbf{S}_b\|}{d_\perp} n_{b,z} n_{b,x} & a^{wv}_{C,b} &= -\frac{\nu \|\mathbf{S}_b\|}{d_\perp} n_{b,z} n_{b,y} & a^{ww}_{C,b} &= \frac{\nu \|\mathbf{S}_b\|}{d_\perp}\left(1 - n^2_{b,z}\right)
\end{aligned} \tag{14}$$

The contribution of the parallel wall velocity still has to be subtracted. This can be done explicitly since the wall velocity is known, yielding

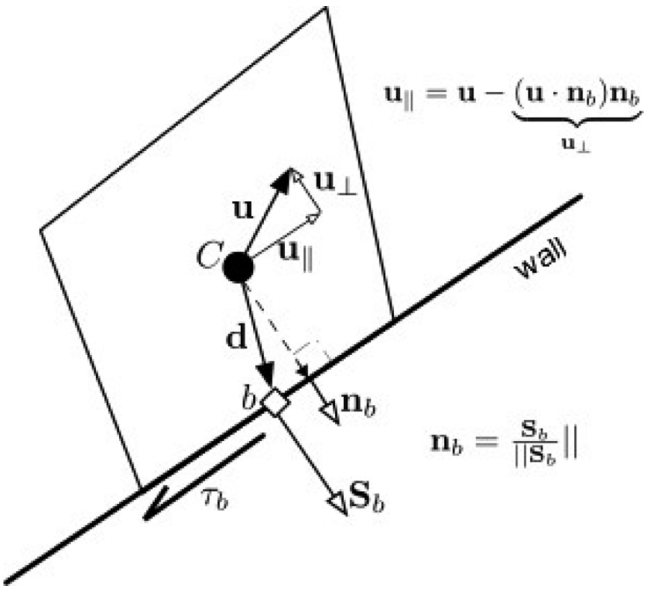

Figure 1. Velocity profile in the near-wall region of a moving wall.

$$b^{u}_{C,b} = \frac{\nu \, \|\mathbf{S}_b\|}{d_\perp} u_{\parallel,wall}$$
$$b^{v}_{C,b} = \frac{\nu \, \|\mathbf{S}_b\|}{d_\perp} v_{\parallel,wall}$$
$$b^{w}_{C,b} = \frac{\nu \, \|\mathbf{S}_b\|}{d_\perp} w_{\parallel,wall} \tag{15}$$

3.3. Cyclic Boundary Conditions

Consider the cyclic boundary condition illustrated in Figure 2. Two patches separated by some angle α are designated to form a periodic connection. For this condition it is usual to have a conforming mesh across the two patches, that is, boundary elements on the side of each of the patches will coincide on a one-to-one basis to those on the other patch.

To obtain a conservative and implicit treatment, the discretization at each of the patch faces proceeds as if the connected element of the other side had been rotated so that it is a neighbor to the patch face under consideration; see Figure 2. In effect, the centroid of the element and the velocity vector attached to it are rotated and the discretization of the patch face can proceed as for any interior face, yielding algebraic coefficients connecting the element across the cyclic patches.

In practice the discretization needs only be carried out on one side of the cyclic patches, generally the master patch, with the coefficients for the other patch element obtained by a rotational transformation. The computed coefficients are then injected into the block matrix at the appropriate position. The result of the discretization, with given transformed geometry, is a preliminary implicit matrix with coefficients $\mathbf{A}_{NB,geom}$. To account for the rotation of vector variables, a rotational transformation is then applied to the implicit coefficients.

$$\mathbf{A}_{NB} = \mathbf{A}_{NB,geom} \cdot \mathbf{T}_{NB} \tag{16}$$

For the pressure velocity system, resulting from the Navier-Stokes equations, we use a 4×4 transformation tensor for the neighboring primitive variables

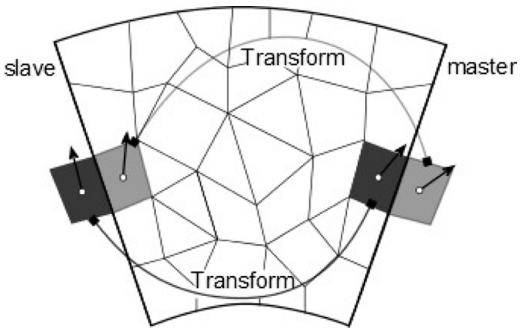

Figure 2. Sketch of a cyclic BC interface.

(**u** and p) that is based on the Rodriguez' formula

$$\mathbf{T}_{NB} = \begin{bmatrix} c(\alpha)+\omega_x^2[1-c(\alpha)] & \omega_x\omega_y[1-c(\alpha)]-\omega_z s(\alpha) & \omega_y s(\alpha)+\omega_x\omega_z[1-c(\alpha)] & 0 \\ \omega_z s(\alpha)+\omega_x\omega_y[1-c(\alpha)] & c(\alpha)+\omega_y^2[1-c(\alpha)] & -\omega_x s(\alpha)+\omega_y\omega_z[1-c(\alpha)] & 0 \\ -\omega_y s(\alpha)+\omega_x\omega_z[1-c(\alpha)] & \omega_x s(\alpha)+\omega_y\omega_z[1-c(\alpha)] & c(\alpha)+\omega_z^2[1-c(\alpha)] & 0 \\ 0 & 0 & 0 & 1 \end{bmatrix} \tag{17}$$

where ω is the unit rotation vector and α is the rotation angle.

3.4. Arbitrary Mesh Interface (AMI)

In OpenFOAM the discretization across an arbitrary mesh interface (AMI) works by constructing on each side of the interface a shadow neighbor cell whose value is computed from the weighted interpolations of the adjacent elements of the cell under consideration; this is best illustrated in Figure 3*b*. Coefficients for each term can be found for each cell–shadow cell pair. In OpenFOAM the shadow cell coefficients are multiplied with their respective interpolated value.

For the coupled solver a different approach was used in that the connection across the interface is treated implicitly. That is, the elements on each side of the

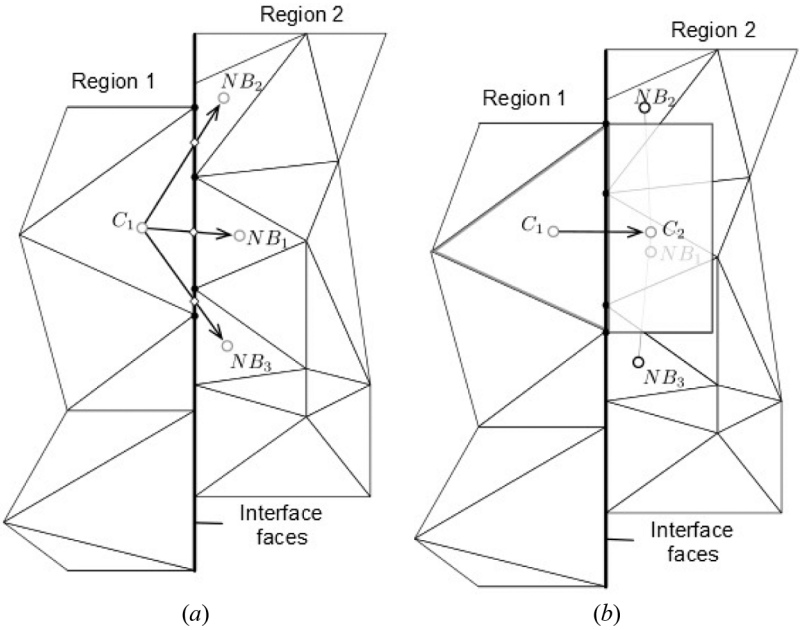

Figure 3. AMI discretization across two regions: (*a*) direct approach; (*b*) shadow cell approach.

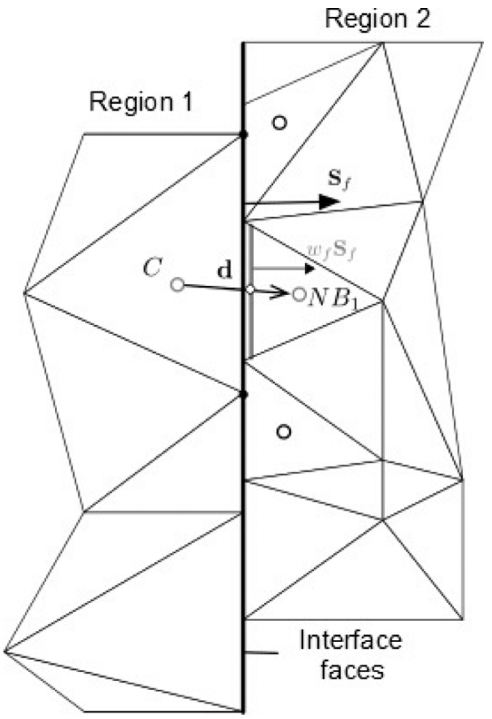

Figure 4. AMI interface close-up.

interface are treated as directly connected through faces that are weighted subsurfaces of their master surface, as seen in Figure 3a.

Taking as example the discretization of the Laplacian pressure term arising in the continuity equation, using the notations depicted in Figure 4 we get by considering a subsurface on the master AMI patch with a weight fraction w_{f_1}

$$-w_{f_1}\mathbf{S}_f \cdot \overline{\mathbf{D}_f} \cdot \nabla p_f = -\frac{w_{f_1}\mathbf{S}_f \cdot \overline{\mathbf{D}_f} \cdot w_{f_1}\mathbf{S}_f}{\mathbf{d} \cdot w_{f_1}\mathbf{S}_f}\left(p_{NB_1} - p_C\right) - \underbrace{\left(w_{f_1}\mathbf{S}_f \cdot \overline{\mathbf{D}_f} - \frac{w_{f_1}\mathbf{S}_f \cdot \overline{\mathbf{D}_f} \cdot w_{f_1}\mathbf{S}_f}{\mathbf{d} \cdot w_{f_1}\mathbf{S}_f}\mathbf{d}\right)}_{\mathbf{N}} \cdot \overline{\nabla p_f} \tag{18}$$

The implicit part, that is the first term on the RHS of Eq. (18), is linearized as

$$a_C^{pp} = w_{f_1}\frac{\mathbf{S}_f \cdot \overline{\mathbf{D}_f} \cdot \mathbf{S}_f}{\mathbf{d} \cdot \mathbf{S}_f} \qquad a_{NB_1}^{pp} = -w_{f_1}\frac{\mathbf{S}_f \cdot \overline{\mathbf{D}_f} \cdot \mathbf{S}_f}{\mathbf{d} \cdot \mathbf{S}_f} \tag{19}$$

while the explicit part is moved to the RHS.

Using this approach we are effectively stitching the various block grids into one set of connected meshes yielding an implicit system of equations. The matrices

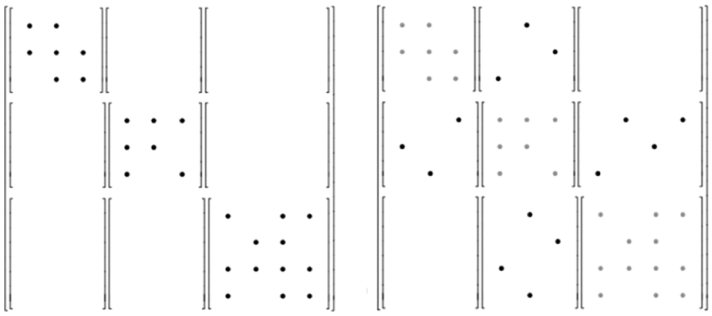

Figure 5. (*a*) Matrix with interior block connections; (*b*) matrix in AMI connections.

resulting from these two operations are shown in Figure 5; more details of the procedure can be found in [7].

A cyclic boundary condition can also have a nonconforming mesh. In this case the discretization proceeds as for a cyclic boundary condition, except for the use of sub-surfaces.

4. SOLUTION PROCEDURE

It is essential to use a multigrid solver to solve the linearized system of equations. A block-coupled multigrid solver using an algebraic correction approach and block-ILU smoothers has been developed for the solution of the given governing equations [1]. In addition to solving the linearized system of equations an outer loop is needed to resolve the non-linearities in these equations. The resulting solution procedure is similar to that depicted in the companion article [1], the difference being an additional update of the relative fluxes. The solution procedure reads

0 - Initialize values for volume flux $\dot{V}^{(n)}$, pressure $p^{(n)}$ and velocities $\mathbf{u}^{(n)}$.
1 - Update volume flux in rotational frame of reference $\dot{V}_r^{(n)}$ using volume flux of absolute frame of reference $\dot{V}^{(n)}$.
2 - Assembles source and matrix coefficients for momentum equations.
3 - Evaluate the **D** tensor field from momentum equations' matrix coefficients.
4 - Assemble source and matrix coefficients for continuity equation.
5 - Solve simultaneously for pressure $p^{(n+1)}$ and velocities $\mathbf{u}^{(n+1)}$.
6 - Solve the turbulence equations sequentially and adapt the kinematic turbulent viscosity ν_t.
7 - Extract absolute volume flux $\dot{V}^{(n+1)}$ from continuity equation.
8 - Return to step 1 and loop until convergence.

5. RESULTS

Three industrial test cases, namely, a pump runner, a Francis turbine runner, and a Kaplan turbine, are used to evaluate the performance of the coupled solver

under MFR conditions. A state-of-the-art OpenFOAM solver developed by Casartelli et al. [15] is used for comparison. For all tests, a k–ω SST turbulence model is used and the simulation is considered converged when the normalized root-mean-square (RMS) residual for each field is smaller than 10^{-5}. The evaluated RMS is defined as

$$RMS(\phi) = \frac{\sqrt{\frac{1}{N}\sum_{i=0}^{N}\left\{res[\phi(i)]/a_C^{\phi\phi}\right\}^2}}{max(\phi,0) - min(\phi,0)} \tag{20}$$

5.1. Pump Runner

The setup for the pump runner test case, as seen in Figure 6, consists of a single-blade channel with cyclic AMI interfaces (Section 3.3). Hub, shroud, and blade are moving with a prescribed absolute velocity, so the shear stress at these patches is treated as outlined in Section 3.2. For these walls a Neumann boundary condition is prescribed for the pressure, while the blended wall functions are used for turbulence quantities. At the inlet, velocity and turbulence quantities are specified, while a Neumann boundary condition is applied to the pressure. For the outlet, a Neumann boundary condition is applied to the velocity and turbulence quantities, while a specified-value condition is used for the pressure field.

The investigated operating point is close to the optimal operating point, and almost no secondary flow occurs inside the runner channel. The pump has a medium specific speed characteristic, and its relatively high deceleration rate makes it an aggressive diffuser.

For validation purposes the velocity profiles evaluated from hub to shroud at the trailing edge computed with the coupled solver were compared to those

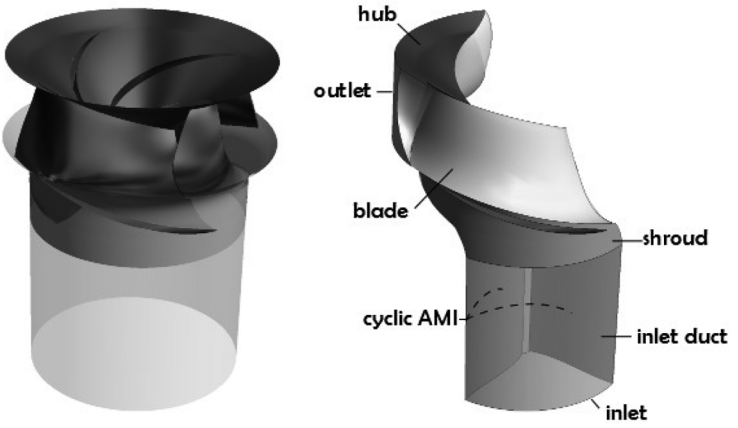

Figure 6. Pump configuration.

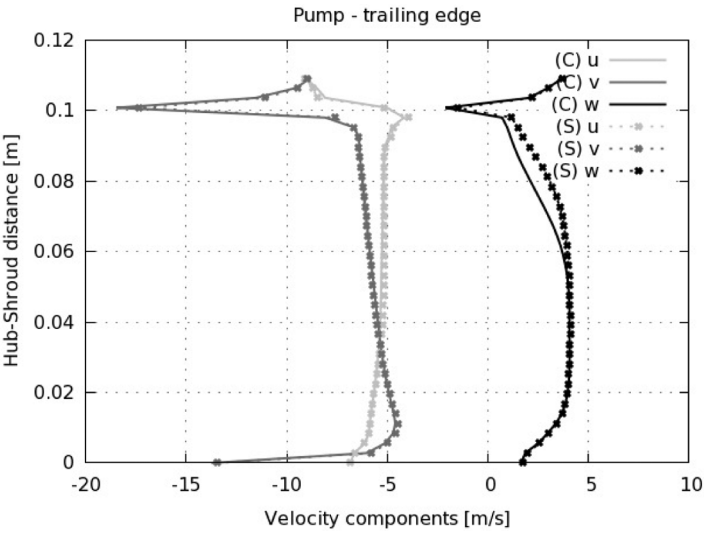

Figure 7. Pump's velocity profiles close to the trailing edge.

computed with the segregated benchmark solver. The profiles in Figure 7 show good conformance.

To evaluate the performance and scalability, three different mesh sizes with increasing numbers of cells are used. Results in Table 1 clearly show that the coupled solver scales nearly linearly with mesh size, while the segregated solver suffers as the number of elements increases. The convergence characteristics can be seen in Table 1 and in Figure 8.

It is worth noting that the segregated solver did not converge to the desired level on the coarsest grid, because of the presence of highly distorted elements. The coupled solver did not encounter such an issue. For the other meshes the coupled solver substantially outperformed the segregated solver.

5.2. Francis Turbine Runner

The Francis turbine test case, depicted in Figure 9, shares many of the boundary conditions of the pump runner case except in the flow direction. Again, only a single-blade channel is modeled with a cyclic AMI interface. The turbine has a relatively high-head, low-debit characteristic, and the flow is being accelerated rather than decelerated (as was the case for the pump runner). This fact should improve the convergence behavior.

Table 1. Pump: Performance comparison of the coupled (C) and segregated (S) algorithms

# CVs	(C) time [s]	(C) time/CV [s]	(S) time [s]	(S) time/CV [s]	S/C
309 k	652.4	0.002111	x	x	x
802 k	2,399.2	0.002991	20,351.7	0.025250	8.48
1,260 k	3,144.5	0.002495	36,360.9	0.028858	11.56

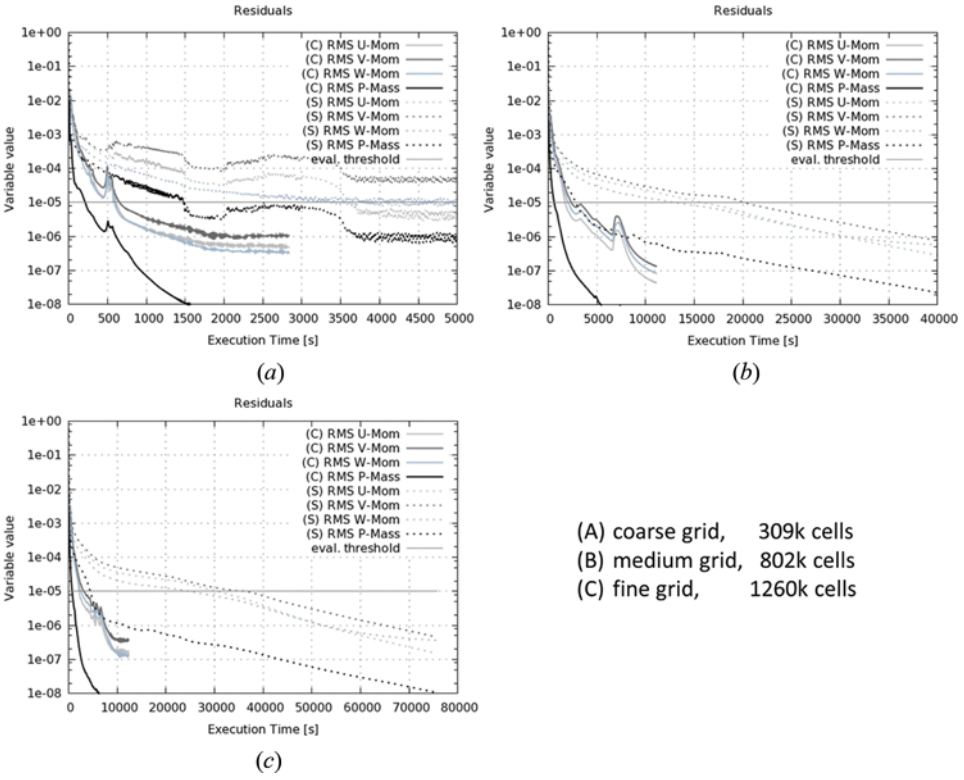

Figure 8. Convergence histories for Pump test case: (a) coarse grid 309k cells; (b) coarse grid 802k cells; (c) coarse grid 1260k cells.

Velocity profiles evaluated from hub to shroud at the trailing edge again show good conformance with respect to the segregated approach (see Figure 10). Small discrepancies for the velocity component in x-direction are very probably due to a small difference in the turbulence treatment, especially at the boundary.

In terms of mesh size scalability, Table 2 indicates again that the coupled solver scales almost linearly, whereas the segregated solver does not. The convergence history can be seen in Figure 12, and convergence results in Table 2.

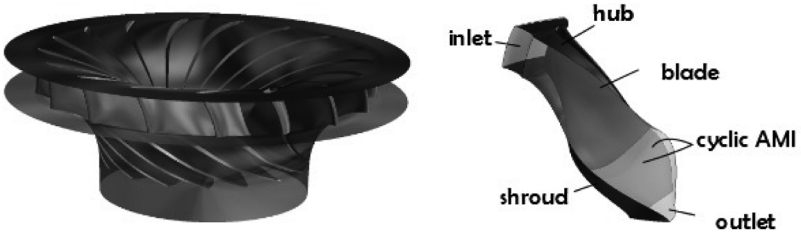

Figure 9. Francis turbine runner configuration.

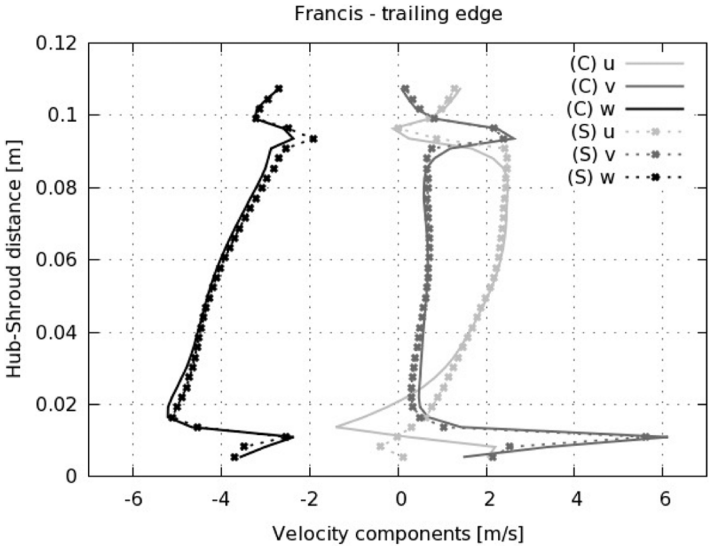

Figure 10. Francis velocity profiles close to the trailing edge.

Figure 11 shows the scaled computational cost of the coupled and segregated solvers. The scale factor is defined as

$$Scale\ factor = \frac{(time/CV)_{nCells}}{(time/CV)_{ref}} \tag{21}$$

and basically represents the convergence computational cost per element.

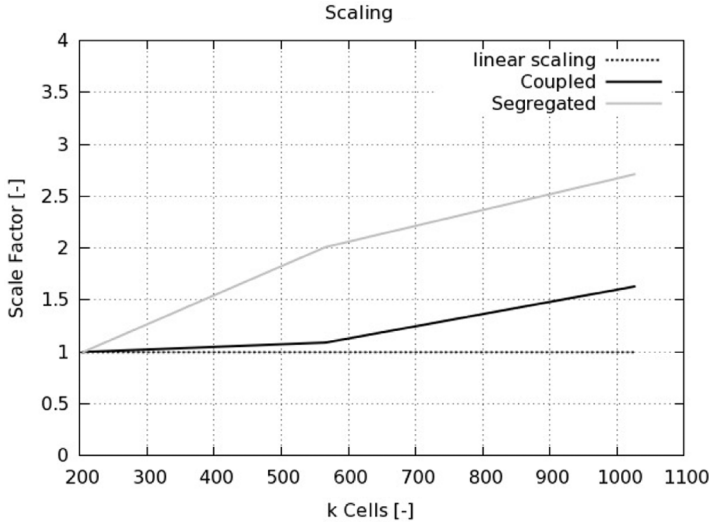

Figure 11. Francis mesh size scaling.

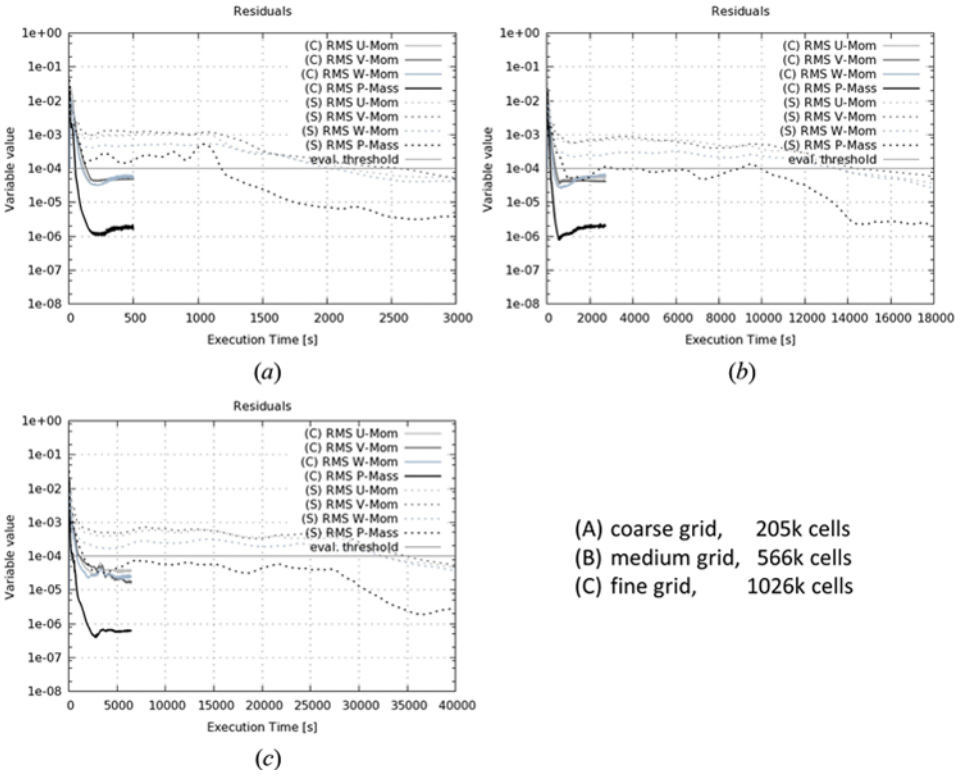

Figure 12. Convergence histories for the Francis test case: (a) coarse grid 205k cells; (b) coarse grid 566k cells; (c) coarse grid 1026k cells.

Figure 12 shows the convergence histories of the coupled and segregated solvers. For the segregated solver the convergence stalls as the mesh size increases, but there is also oscillatory behavior indicating low robustness. This could be due to a variety of causes related to the mesh quality, such as increasing nonorthogonality, and higher aspect ratios.

5.3. Kaplan Turbine

The Kaplan turbine test is a multiblock mesh. This is so to allow for better treatment of the gaps that exist between the hub and the inner part of the blades,

Table 2. Francis: Performance comparison of the coupled (C) and segregated (S) algorithms

# CVs	(C) time [s]	(C) time/CV [s]	(S) time [s]	(S) time/CV [s]	S/C
205 k	136.2	0.000665	2,568.9	0.012543	18.86
566 k	411.4	0.000726	14,442.5	0.025499	35.11
1,026 k	1,109.8	0.001082	34,936.7	0.034051	31.48

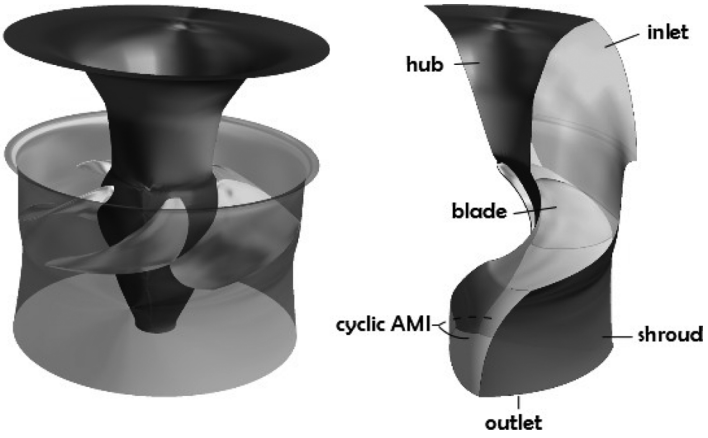

Figure 13. Kaplan turbine configuration.

as well as between the shroud and the outer part of the blades. These gaps are meshed separately and the meshes are subsequently connected to the main part of the computational domain, which comprises a circumferential horizontal intake, the blade region, and the outlet region. The gaps and the main part of the mesh are connected with nonconformal AMI interfaces (as outlined in Section 3.4). The setup for the Kaplan simulation is shown in Figure 13. To retain the good convergence behavior and robustness of the coupled solver, it was critical that the discretization at these nonconformal interfaces be done implicitly and in a way that enforces mass conservation across the interfaces. These issues and the high aspect ratio of the mesh rendered this a very demanding test. Because of the rotational

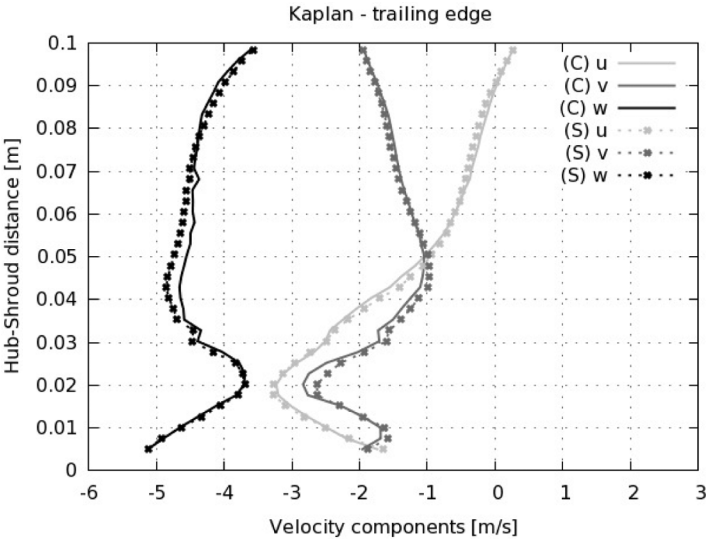

Figure 14. Kaplan velocity profiles close to the trailing edge.

Table 3. Kaplan: Performance comparison of the coupled (C) and segregated (S) algorithms

# CVs	(C) time [s]	(C) time/CV [s]	(S) time [s]	(S) time/CV [s]	S/C
275 k	960.7	0.003489	5,840.6	0.021215	6.08

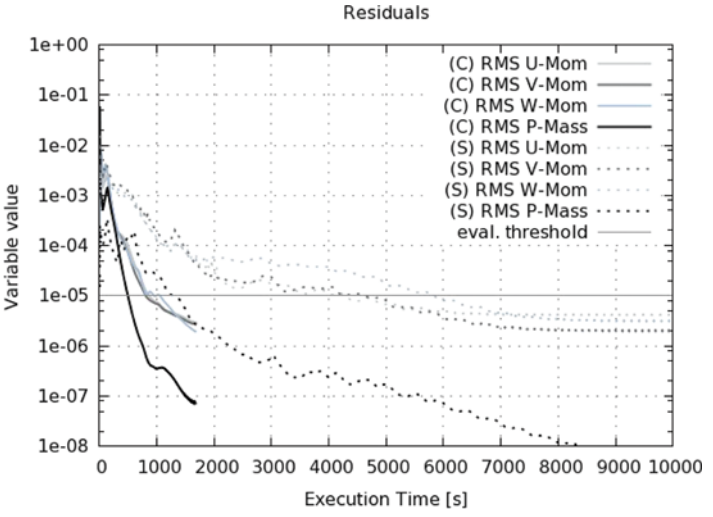

Figure 15. Convergence histories for the Kaplan test case.

symmetry, only one blade channel was modeled through the use of cyclic AMI interfaces.

Velocity profiles evaluated from hub to shroud at the trailing edge again show good conformance with respect to the segregated approach (see Figure 14).

For this test case the coupled and segregated methods are only compared on a single grid. Table 3 and Figure 15 again prove the superiority of the coupled solver over the segregated solver.

The fast convergence rate of the coupled solver for the Kaplan test case and its relative smoothness in convergence indicate that in addition to its excellent performance, the solver is also very robust. This is due to both the strong interequation and intercomponent coupling and to the fully implicit treatment of the coupled interfaces (cyclic AMIs).

5.4. Test Case Summary

The results of the three test cases are summarized in Table 4. Column 2 shows the increase in mesh size for the Pump and Francis cases, normalized in terms of the coarsest mesh. Columns 3 and 4 show the computational cost per control volume (CV) of solving the respective test cases for coupled and segregates solvers respectively for the various mesh sizes. Finally column 5 shows the relative

Table 4. Test case summary of mesh size scaling for coupled (C) and segregated (S) algorithms

Test case	Grid incr. factor	(C) time/CV [s]	(S) time/CV [s]	S/C
Pump	1	0.002111	x	x
	2.60	0.002991	0.025250	8.48
	4.08	0.002495	0.028858	11.56
Francis	1	0.000665	0.012543	18.86
	2.76	0.000726	0.025499	35.11
	5.00	0.001082	0.034051	31.48
Kaplan	1	0.003489	0.021215	6.08

computational cost in terms of cpu time for the segregated solver with respect to the coupled solver.

For the pump test case the mesh increases fourfold while the computational cost of obtaining a solution per control volume for the coupled solver is shown to scale linearly with a nearly constant computational time/CV, the time/CV increases from 0.0021 to 0.0025 that is by about 20%. In the Francis test the mesh increases by a factor of 5. The associated increase in time/CV for the coupled solver scales 62% while for the segregated solver the increase is by 270%. This is translated by an increase in the relative cost of the segregated to the coupled solver from 18 to nearly 31 times.

6. CONCLUSION

In this second article, a set of test cases involving multiple reference frames and multiblock meshes were solved using a novel coupled solver, and results were compared with those obtained using a state-of-the-art segregated solver. As for the stationary test cases of the companion article [1], the coupled solver substantially outperforms the segregated solver and demonstrates mesh scalability. In the context of a multiblock mesh with MRF, this level of performance is achieved by judiciously addressing a number of numerical issues related to the linearization and implicit treatment of boundary and interface conditions. Also worth noting is the convergence characteristics of the coupled solver that are devoid of oscillatory behavior, this is, in the view of the authors, a strong indication as to the robustness of the numerical approach.

FUNDING

Financial aid granted by the Austrian research fund FFG, for projects 828688 - HydroSim and M1543-N30, is greatly acknowledged. Lise Meitner project N. M1466-N30 support is greatly acknowledged as well.

REFERENCES

1. L. Mangani, M. Buchmayr, and M. Darwish, Implementation and Evaluation of a Fully Coupled Solver in OpenFOAM: Steady State Incompressible Turbulent Flows, *Numer. Heat Transfer B*, vol. 66, no. 1, 2014.
2. S. Patankar and D. Spalding, A Calculation Procedure for Heat, Mass and Momentum Transfer in Three-Dimensional Parabolic Flows, *Heat and Mass Transfer*, vol. 15, pp. 1787–1806, 1972.

3. Y. G. Laia, An Unstructured Grid Method for a Pressure-Based Flow and Heat Transfer Solver, *Numer. Heat Transfer B*, vol. 32, no. 3, pp. 267–281, 1997.
4. P. L. Woodfield, K. Suzuki, and K. Nakabe, Performance of a Three-Dimensional, Pressure-Based, Unstructured Finite-Volume Method for Low-Reynolds-Number Incompressible Flow and Wall Heat Transfer Rate Prediction, *Numer. Heat Transfer B*, vol. 43, no. 5, pp. 403–423, 2003.
5. C. Vradis and K. J. Hammad, Strongly Coupled Block-Implicit Solution Technique for Non-Newtonian Convective Heat Transfer Problems, *Numer. Heat Transfer B*, vol. 33, no. 1, pp. 79–97, 1998.
6. M. J. S. de Lemos, Flow and Heat Transfer in Rectangular Enclosures Using a New Block-Implicit Numerical Method, *Numer. Heat Transfer B*, vol. 37, no. 4, pp. 489–508, 2000.
7. M. Darwish, W. Geahchan, and F. Moukalled, Fully Implicit Coupling for Non-Matching Grids, Int. Conf. of Numerical Analysis and Applied Mathematics (ICNAAM 2010), Rhodos, Greece, pp. 47–50, 2010.
8. F. Menter, M. Kuntz, and R. Langtry, Ten Years of Industrial Experience with the SST Turbulence Model, in K. Hanjalic et al. (eds.), *Turbulance Heat and Mass Transfer 4*, Begell House, Inc., 2003.
9. W. Hauger, W. Schnell, and D. Gross, *Technische Mechanik 3*, Springer-Verlag, Berlin, 2002.
10. C. Hirsch, *Numerical Computation of Internal and External Flows*, John Wiley, New York, 1991.
11. A. Hellsten, Some Improvements in Menter's K-Omega SST Turbulence Model, AIAA Paper 98–2554, 1998.
12. P. E. Smirnov and F. R. Menter, Sensitization of the SST Turbulence Model to Rotation and Curvature by Applying the Spalart-Shur Correction Term, *ASME J. Of Turbomachinery*, vol. 131, 2009.
13. M. Darwish and F. Moukalled, A Review of Boundary Conditions and Their Implementations in CFD Codes, Technical Report, 2000.
14. M. Darwish, W. Geahchan, and F. Moukalled, Fully Implicit Coupling for Non-Matching Grids, *Numer. Heat Transfer*, ICNAAM 2010, Crete, Greece, 2010.
15. E. Casartelli, L. Mangani, and S. Hug, Numerical Comparison Between Model and Prototype Flow in a Pump-Turbine Distributor, Int. Conf. and Exhibition Innovative Approaches To Global Challenges, Bilbao, Spain, 2012.